



## Investigation of highly luminescent inorganic perovskite nanocrystals synthesized using optimized ultrasonication method

Sang Yoon Lee<sup>a,b</sup>, Seong Hyun Jang<sup>a,c</sup>, Geonho Lee<sup>a,d</sup>, No-hyung Park<sup>a</sup>, Jongwook Park<sup>d</sup>, Dong Hyup Park<sup>e</sup>, Kwan Hyun Cho<sup>f,\*</sup>, Jae Woong Jung<sup>b,\*</sup>, Jun Choi<sup>a,\*</sup>

<sup>a</sup> Material & Component Convergence R&D Department, Korea Institute of Industrial Technology (KITECH), Ansan 15588, Republic of Korea

<sup>b</sup> Department of Advanced Materials Engineering for Information & Electronics, KyungHee University, Yongin 17104, Republic of Korea

<sup>c</sup> Lab. Of Organic Photo-functional Materials, Department of Materials Science and Engineering, Seoul National University, Seoul 08826, Republic of Korea

<sup>d</sup> Department of Chemical Engineering, KyungHee University, Yongin 17104, Republic of Korea

<sup>e</sup> Applied Polymer Research Center, Korea Conformity Laboratories, Incheon 21594, Republic of Korea

<sup>f</sup> Digital Transformation R&D Department, Korea Institute of Industrial Technology (KITECH) Ansan 15588, Republic of Korea

### ABSTRACT

All-inorganic halide perovskite nanocrystals are next-generation materials with excellent optical and semiconductor properties suitable for display applications. In this study, we introduce an optimized ultrasonication method for the high-capacity synthesis of highly luminescent inorganic perovskite nanocrystals. After the synthesis of CsPbBr<sub>3</sub> with superior optical performance by ultrasonication method, halide anion exchange was performed to tune the stable emission wavelength over the entire visible range. In particular, the maximum photoluminescence wavelengths of the red and green perovskite nanocrystals were appropriate for light-emitting diode applications, and their full-width-at-half-maximum were very narrow, showing outstanding color purity. The materials also had excellent thermal and photostability, which is a necessary requirement for perovskite nanocrystal/organic light-emitting diode hybrid device applications. We formulated uniformly stable perovskite nanocrystal inks and optimized their physical and rheological properties for successful inkjet-printing. Finally, we fabricated a hybrid device with a color conversion layer based on the red and green perovskite nanocrystals synthesized using the optimized ultrasonication and halide-ion-exchange methods. The color reproduction range of the fabricated devices was 27.3 % wider than that of the National Television System Committee values, indicating very vivid colors.

### 1. Introduction

Perovskite materials are being actively studied as optoelectronic materials because of their outstanding properties. In particular, perovskite nanocrystals (PeNCs) have high absorption coefficients, high photoluminescence quantum yields (PLQY), and excellent color purity owing to the narrow full-width-at-half-maximum (FWHM) of the photoluminescence wavelength [1]. One of the most important properties of PeNCs is that the band gap can be easily tuned by adjusting the ratio of halide elements. The outstanding optoelectronic properties of inexpensive and solution-processable lead-halide PeNCs have brought them to the forefront of many research fields, such as the development of solar cells [2,3], light emitting diodes (LEDs) [4–6], photodetectors [7,8], lasers [9], and semiconductors [10,11]. Their initial research was focused on organic/inorganic hybrid materials, but all-inorganic materials quickly gained priority because of their higher stability. Furthermore, the solution processing of PeNCs has a much higher chemical state stability than conventional two-dimensional thin-film deposition processes [12].

Currently, unlike conventional metal-chalcogenide-based quantum dots (QDs), there are only few synthesis methods available for the preparation of PeNCs. The synthesis methods are classified into two main types. The most widely adopted method for the preparation of PeNCs with excellent optoelectronic properties are based on high-temperature hot injection [13–16]. However, because this method is somewhat complicated and must be performed in an inert atmosphere, it has only been studied on a small scale. The second method is ligand-assisted reprecipitation (LARP), which provides easier synthesis at room temperature [17]. Despite its advantages, the perovskite precursors obtained from the LARP method generally have poor optical and structural properties because they are highly susceptible to highly polar solvents [18]. Therefore, a silica oxide passivation method was developed where PeNCs are coated with a silica shell to ensure their long-term and moisture stability [19,20]. These two methods are not considered suitable for high-capacity commercial production of PeNCs, and now there is a growing demand for superior methods suitable for high-volume production.

Hence, we developed an optimized ultrasonication method for the

\* Corresponding authors.

E-mail addresses: [khcho@kitech.re.kr](mailto:khcho@kitech.re.kr) (K.H. Cho), [wodndwdj@khu.ac.kr](mailto:wodndwdj@khu.ac.kr) (J.W. Jung), [skywork1@kitech.re.kr](mailto:skywork1@kitech.re.kr) (J. Choi).

<https://doi.org/10.1016/j.ultsonch.2022.106145>

Received 10 July 2022; Received in revised form 22 August 2022; Accepted 25 August 2022

Available online 28 August 2022

1350-4177/© 2022 The Authors. Published by Elsevier B.V. This is an open access article under the CC BY-NC-ND license (<http://creativecommons.org/licenses/by-nc-nd/4.0/>).

high-capacity synthesis of highly luminescent inorganic PeNCs. The ultrasonic method in this study is a room-temperature strategy, and it avoids the use of polar toxic solvents and does not require inert conditions. After the high-capacity synthesis of CsPbBr<sub>3</sub> NCs with high PLQY by the ultrasonication method, halide-ion exchange (HIE) was performed to tune the stable emission wavelength. These combined methods were able to synthesize PeNCs with emission in the entire visible color range easily and quickly with high efficiency in mild conditions. In addition, the prepared PeNCs were evaluated for use as the color conversion layer (CCL) of quantum dot organic light-emitting diode (QD/OLED) displays. Such devices provide excellent display performance and are suitable for industrial scale production. Their color reproducibility can be improved by adding QD CCLs on top of the blue OLED light source [6,21]. Thus, PeNCs which have solution processability and superior optical properties compared to conventional QD materials, were used as CCLs, and applied as PeNCs/OLED devices. The ultrasonically synthesized PeNCs were appropriately formulated into inks for inkjet-printing of device components, and then photocured after pixel patterning on a substrate on which a black pixel bank was formed. Compared to other patterning methods, inkjet-printing can remarkably reduce the number of processing steps and material consumption, while facilitating the production of large-area panels and eco-friendly production systems [22,23]. The wettability of the substrate and ink ejection properties of the prepared PeNC inks were also optimized and compared with the performance of existing results [6,21].

## 2. Experimental section

### 2.1. Materials

Cesium carbonate (Cs<sub>2</sub>CO<sub>3</sub>, 99 %), Lead(II) bromide (PbBr<sub>2</sub>, ≥98 %), lead(II) iodide (PbI<sub>2</sub>, 99.999 %), lead(II) Chloride (PbCl<sub>2</sub>, 98 %), 1-octadecene (ODE, 90 %), oleic acid (OA, 95 %), oleylamine (OAm), hexane anhydrous (95 %), toluene anhydrous (99.8 %), isobornyl acrylate, dipentaerythritol penta-/hexa-acrylate, diphenyl(2,4,6-trimethylbenzoyl) phosphine oxide, IGEPAL 520, IGEPAL 630, diethylene glycol (99 %), triethylene glycol (99 %), glycerol (≥99 %), propylene glycol monoether acetate (PGMEA, ≥9.5), and molybdenum trioxide (MoO<sub>3</sub>, 99.97 %) from Sigma-Aldrich were used without additional purification. N,N-bis(naphthalen-1-yl)-N,N-bis(phenyl)benzidine (NPB), tris(4-carbazoyl-9-ylphenyl)amine (TCTA), N,N'-dicarbazoyl-3,5-benzene (mCP), bis[2-(4,6-difluorophenyl)pyridinato-C<sub>2</sub>,N](picolinato)iridium(III) (FIrpic), 2,2,2'-(1,3,5-benzinetriyl)-tris(1-phenyl-1-H-benzimidazole) (TPBI), and lithium fluoride (LiF) (1 nm) were purchased from OSM. Aluminum (Al) and silver (Ag) were obtained from TASCOC. Indium-tin oxide (ITO) was purchased from GUNZE [6,21].

### 2.2. Ultrasonic synthesis of CsPbBr<sub>3</sub> perovskite nanocrystals

Cs<sub>2</sub>CO<sub>3</sub> (0.03258 g, 0.1 mmol), PbBr<sub>2</sub> (0.1101 g, 0.3 mmol), ODE (10 mL), OA (0.5 mL) and OAm (0.5 mL) were loaded into 20 mL vial and stirring for 10 min. Then the reaction mixture was subjected to ultrasonication treatment at a power of 70 W and an amplitude 90 % for 3.5 min. During the reaction process, it can be clearly seen that the color of the reaction solution changes from colorless to greenish yellow indicating the formation of green perovskite NCs. And they exhibit strong fluorescence emission upon UV light excitation. After the reaction, the reaction mixture was rapidly cooled to room temperature and centrifuged at 12,000 rpm for 10 min. After that, the collected precipitate was dispersed in hexane (10 mL) and centrifuged at 12,000 rpm for 10 min and a supernatant was obtained.

### 2.3. Ion exchange method (for red perovskite nanocrystals)

PbI<sub>2</sub> 120 mg, OA 70 μL and OAm 70 μL were loaded into vial and stirring for 1 min. Then, add 3 mL of green perovskite nanocrystals

solution and vigorously stirred to initiate the reaction. The reaction temperature was maintained at 50 °C. Then, the wavelength is adjusted according to the stirring time (orange PeNC 5 min and red PeNC 10 min). When the desired wavelength is reached, the reaction is terminated and centrifuged at 10,000 rpm for 1 min. After that, the collected precipitate was dispersed in hexane 1 mL.

### 2.4. Ion exchange method (for blue perovskite nanocrystals)

PbCl<sub>2</sub> 90 mg, OA 140 μL and OAm 70 μL were loaded into vial and stirring for 1 min. Then, add 3 mL of green perovskite nanocrystals solution and vigorously stirred to initiate the reaction. Then, the wavelength is adjusted according to the stirring time (cyan PeNC 30 min and blue PeNC 60 min). When the desired wavelength is reached, the reaction is terminated and centrifuged at 10,000 rpm for 1 min. After that, the collected precipitate was dispersed in hexane 1 mL.

### 2.5. Ink formulation

Perovskite nanocomposite inks for inkjet-printing were prepared with post-treated PeNCs solution, toluene, and the photocurable resin in a ratio of 1:2:4. The photocurable resin used herein was composed of isobornyl acrylate, dipentaerythritol hexaacrylate, and diphenyl (2,4,6-trimethylbenzoyl) phosphine oxide monomers in a ratio of 2:1:1, respectively. The Irgacure series photoinitiator was composed of 2 wt% of the total ink weight. IGEPAL 520 and IGEPAL 630 were also included in a ratio of 8:2 as the surfactants forming 5 wt% of the total resin weight. Diethylene glycol, triethylene glycol, and glycerol comprised 6–8 wt% of the total resin weight to attain the optimal rheological properties required for the inkjet-printing process.

### 2.6. PeNC/OLED device fabrication

We fabricated a hybrid PeNCs/OLED device by combining the blue OLED and inkjet-printed red/green PeNC CCLs. Firstly, we fabricated a top-emitting blue OLED considering the microcavity effect. To fabricate the blue OLEDs, a glass substrate was cleaned by sonication in distilled water for 40 min, in acetone for 40 min and in IPA for 40 min. All organic and metal layers were deposited by thermal evaporation under a vacuum atmosphere of  $3 \times 10^{-7}$  Torr. The blue OLED devices consisted of a stacked structure of Al (100 nm) as an anode, MoO<sub>3</sub> (5 nm) as a hole injection layer, NPB (20 nm) as a hole injection layer, TCTA (15 nm) as a hole transport layer, mCP and 16 wt% FIrpic as the host/dopant for the blue emitting layer (30 nm), TPBi (25 nm) as an electron transport layer, LiF (1 nm) as an electron injection layer, Al (1 nm) and Ag (15 nm) as cathode electrodes, and NPB (60 nm) as the capping layer. The inkjet-printing was performed with a Dimatix printer equipped with a 10 pl volume head under the conditions of 19 V and 1 kHz. More than 12 ink drops were stacked into the black bank-patterned pixels on the glass substrate. The width of the patterned pixels was 174 μm, the length was 50 μm, and the black bank height was 5.4 μm.

### 2.7. Characterization

The synthesis of PeNCs was treated with Badelin SONOPLUS Digital Ultrasonic Homogenizer set (A. SONOPLUS HD 2070.2 Set). Transmission Electron Microscope (TEM) was conducted with a JEOL JEM-2100F. X-ray Diffraction (XRD) was obtained by a PANalytical Empyrean Alpha-1 X-ray diffractometer. Photoluminescence (PL) spectra, diurnal variations and thermal variations were investigated using a Scinco FS-2 fluorescence spectrometer. Ultraviolet/Visible (UV/Vis) Absorption spectra were measured using a Scinco Mega-800 UV/Vis spectrometer. Time-Resolved Photoluminescence (TRPL) measurements were carried out using the TRPL-FS5 from Edinburgh Instruments. The size and depth of the patterned pixels were measured with a VHX-6000 digital microscope (Keyence, Japan) and an alpha-step D-500 (KLA, US),

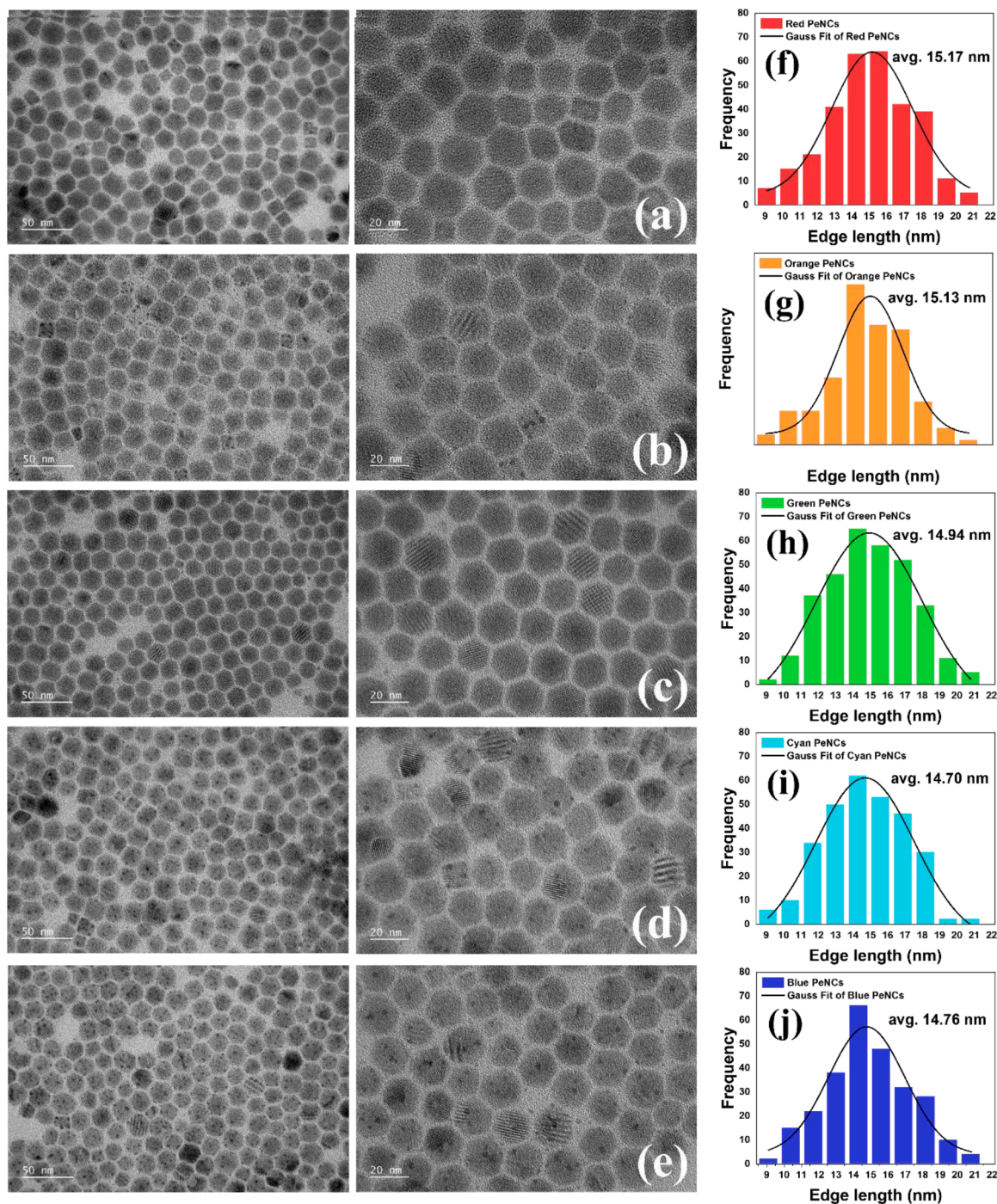


**Fig. 1.** (a–e) TEM images of the synthesized PeNCs: (a) red, (b) orange, (c) green, (d) cyan and (e) blue, and (f–j) size distribution of PeNCs: (f) red, (g) orange, (h) green, (i) cyan and (j) blue.

respectively. The PLQY and FWHM were collected using an Absolute PL Quantum yield spectrometer Quantaury-QY. The excitation wavelength for PLQY and PL lifetime measurements is 365 nm. Inkjet-printing tests and jetability tests were conducted using a Dimatix Printer DMP-2800 and a DMC-11610 cartridge (Fujifilm Co., Japan). Viscosity values were obtained by a Brookfield Programmable Digital Viscometer DV-II + Pro LV. Contact angle values were collected using a KRUSS Co. DSA100. The current–voltage–luminance (J–V–L) characteristics of the PeNCs/OLED hybrid display device and color coordinates were conducted using M6100 OLED J–V–L test system.

### 3. Results and discussion

Detailed proof of the high quality of the synthesized PeNCs by ultrasonication method and HIE was obtained by TEM image analysis. Except for the green CsPbBr<sub>3</sub> NCs, the other color PeNCs were obtained by combined (ultrasonication and HIE) method. The TEM images in Fig. 1a–e show the synthesized CsPbBr<sub>3</sub> and ion-exchanged PeNCs that had various emission colors. The average crystal sizes were in the range of 14–15 nm from the red to blue PeNCs (Fig. 1f–j). The prepared CsPbBr<sub>3</sub> PeNCs were monodisperse, with an average size of 14.94 nm. The average size of red PeNCs ion-exchanged with PbI<sub>2</sub> increased slightly with HIE treatment time, and the average size of blue PeNCs ion-

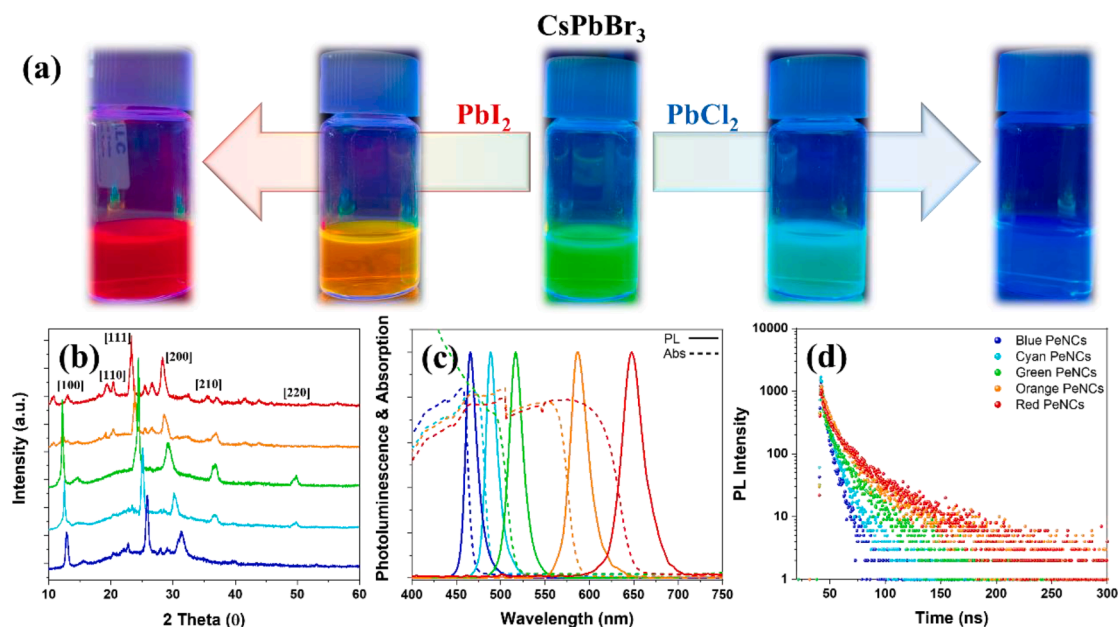


Fig. 2. The characterization of the prepared PeNCs solutions with different halide compositions: (a) The photographs under UV light illumination, (b) The XRD patterns, (c) The UV/Vis absorption spectra (dash line) and PL spectra (solid line), and (d) The TRPL decay curves.

exchanged with  $\text{PbCl}_2$  decreased with HIE treatment time. This difference in the average particle size was due to the different sizes of the exchanged halide ions. The ionic radius of  $\text{Br}^-$  ions is 1.96 Å, that of  $\text{I}^-$  ions is 2.20 Å, and that of  $\text{Cl}^-$  ions is 1.81 Å. Therefore, red shift PeNCs exchanged with  $\text{I}^-$  ions have a larger particle size, and blue shift PeNCs exchanged with  $\text{Cl}^-$  ions have a smaller particle size [24]. The TEM images show the  $\text{CsPbBr}_3$  and various ion-exchanged PeNCs had a hexagonal shape rather than the typical square shape. This difference arises from our optimized ultrasonication synthesis method for mass production. This method is based on the formation of metal–ligand complexes under ultrasonication. During the experiment,  $\text{PbBr}_2$  was decomposed by OA and dissolved into ODE  $\text{Pb}^{2+}$ ,  $\text{Br}^-$ ,  $\text{PbBr}_3^-$ , and  $\text{PbBr}_4^{2-}$ . These ions react with dissolved  $\text{Cs}^+$  ions and form a thin layer of yellowish-orange  $\text{CsPbBr}_3$  on their surface via fast interfacial reactions [13,25]. When sonication begins, the remaining salts with interfacial  $\text{CsPbBr}_3$  are broken down into smaller pieces by ultrasonic forces and completely dissolve within 1 min. As the  $\text{PbBr}_4^{2-}$  concentration reaches a critical level of over-saturation, the nuclei of  $\text{CsPbBr}_3$  spontaneously form near the ultrasonic bubbles and grow into micro- and submicron crystals via  $\text{Cs}^+(\text{sol}) + \text{PbBr}_4^{2-}(\text{sol}) \rightarrow \text{CsPbBr}_3(\text{s}) + \text{Br}^-(\text{sol})$  [13,25]. The growth of NCs ceased after approximately 3 min of ultrasonication treatment. This specificity can form hexagonal PeNCs, which are different from the typical square crystals. It was found that the PL behavior of hexagonal PeNCs is usually better than that of typical square-shaped PeNCs [26]. These characteristics can be analyzed indirectly by density functional theory (DFT) calculation etc. [27].

Based on  $\text{CsPbBr}_3$  synthesized by ultrasonication, other PeNCs with different emission wavelengths were obtained by time controlled HIE (Fig. 2a). The degree of HIE was controlled by the reaction time to achieve PeNCs with the desired emission color. HIE with  $\text{PbI}_2$  took approximately 5 min to produce orange PeNCs (585 nm) and 10 min to produce red PeNCs (647 nm). Ion exchange with  $\text{PbCl}_2$  took approximately 1 h to produce cyan PeNCs (489 nm) and 2 h to produce blue PeNCs (464 nm). The HIE times were determined according to the degree of ionization of each lead halide compound. The ionization potentials (IPs) from a previous report were used: 10.02 eV for  $\text{PbCl}_2$  and 8.82 eV for  $\text{PbI}_2$  [28]. Therefore, the HIE reaction time should be longer for  $\text{PbCl}_2$ . After optimization of the HIE method, the XRD patterns were analyzed to confirm the structure of the synthesized PeNCs with various emission colors (Fig. 2b). Not only the  $\text{CsPbBr}_3$  PeNCs synthesized by

Table 1

The PLQY value, the peak wavelength, and the FWHM of the prepared PeNC solutions.

Sample	Maximum PL wavelength (nm)	PLQY (%)	FWHM (nm)
Red PeNCs	647	82.0	30.34
Orange PeNCs	585	46.8	27.32
Green PeNCs	518	88.4	18.03
Cyan PeNCs	489	33.3	17.68
Blue PeNCs	464	17.7	15.31

optimized ultrasonication but also the ion-exchanged red, orange, cyan, and blue PeNCs at room temperature showed the traditional cubic crystal structure of perovskite materials [29,30]. The size and shape of the  $\text{CsPbBr}_3$  PeNCs were also preserved during HIE. However, the XRD pattern of the prepared PeNC showed a slight angular shift due to the lattice structure change owing to the aforementioned ion size effect. The optical properties of the ultrasonically synthesized PeNCs before and after halide ion exchange were analyzed using UV/Vis absorption and PL spectroscopy (Fig. 2c). The absorption and PL spectra of the prepared PeNC solution were gradually blue-shifted with increasing chloride content and red-shifted with increasing iodide content. Thus, the optical bandgap and PL spectra of the prepared PeNCs were tunable across the full visible range. As shown in Table 1, the maximum PL wavelengths of the red and green PeNCs after the ion exchange reaction were appropriate for LED applications, and their FWHMs were very narrow, showing outstanding color purity.  $\text{CsPbBr}_3$  PeNCs synthesized by the ultrasonication method showed an excellent PLQY value of 88.4 %. This is similar to previously published results and is a remarkable result considering that it is not passivated at all [6,30,31]. The prepared PeNC solutions containing major  $\text{I}^-$  ions had relatively high PLQY values (~82 %), whereas the major  $\text{Cl}^-$ -containing samples had low PLQY values of approximately 17 %. Improving the optical properties of blue perovskites is a major challenge in various perovskite LED researches [32–34]. TRPL was also performed to compare the exciton recombination dynamics of the prepared PeNC solutions, as shown in Fig. 2d. The PL decay curves were fitted based on biexponential decay. The average PL lifetimes of the prepared PeNC solutions showed the same trend as that of halide-composition-dependent TRPL decay for conventional PeNCs [13]. Recent studies have shown that this is mostly attributable to

**Table 2**

The summary of the parameters from the TRPL decay data of the prepared PeNC solutions.

Sample	$\tau_1$ (ns)	$\tau_2$ (ns)	$\tau_{\text{avg}}$ (ns)
Red PeNCs	3.729	26.371	19.976
Orange PeNCs	5.787	25.017	15.363
Green PeNCs	1.911	15.175	11.281
Cyan PeNCs	1.807	8.338	5.636
Blue PeNCs	2.275	7.691	4.745

differences in nonadiabatic charge-phonon coupling [35–37]. A concomitant increase in the radiative decay rate from iodide to bromide to chloride results in a further increase in PL decay [37]. As shown in

**Table 2**, red PeNCs had the longest PL lifetime of 19.976 ns, followed by orange, green, cyan, and blue PeNCs in descending order. The excellent optical properties, high PLQY, and stable PL lifetime of the PeNCs with various colors prepared using the optimized ultrasonication method in this study imply that they can be used for high-capacity PeNC synthesis and PeNC/OLED hybrid devices.

To investigate the stability of the prepared PeNCs under various conditions, their PL intensities were measured over time (**Fig. 3**). The PeNC films for stability measurements were prepared uniformly by individual spin-coating of PeNC solutions at 2,000 rpm for 1 min. The continuous PL intensity of the red, green, and blue (RGB) samples over 28 days was plotted in **Fig. 3a**. After measurements on the first, second, fourth, and seventh days, measurements were performed at weekly

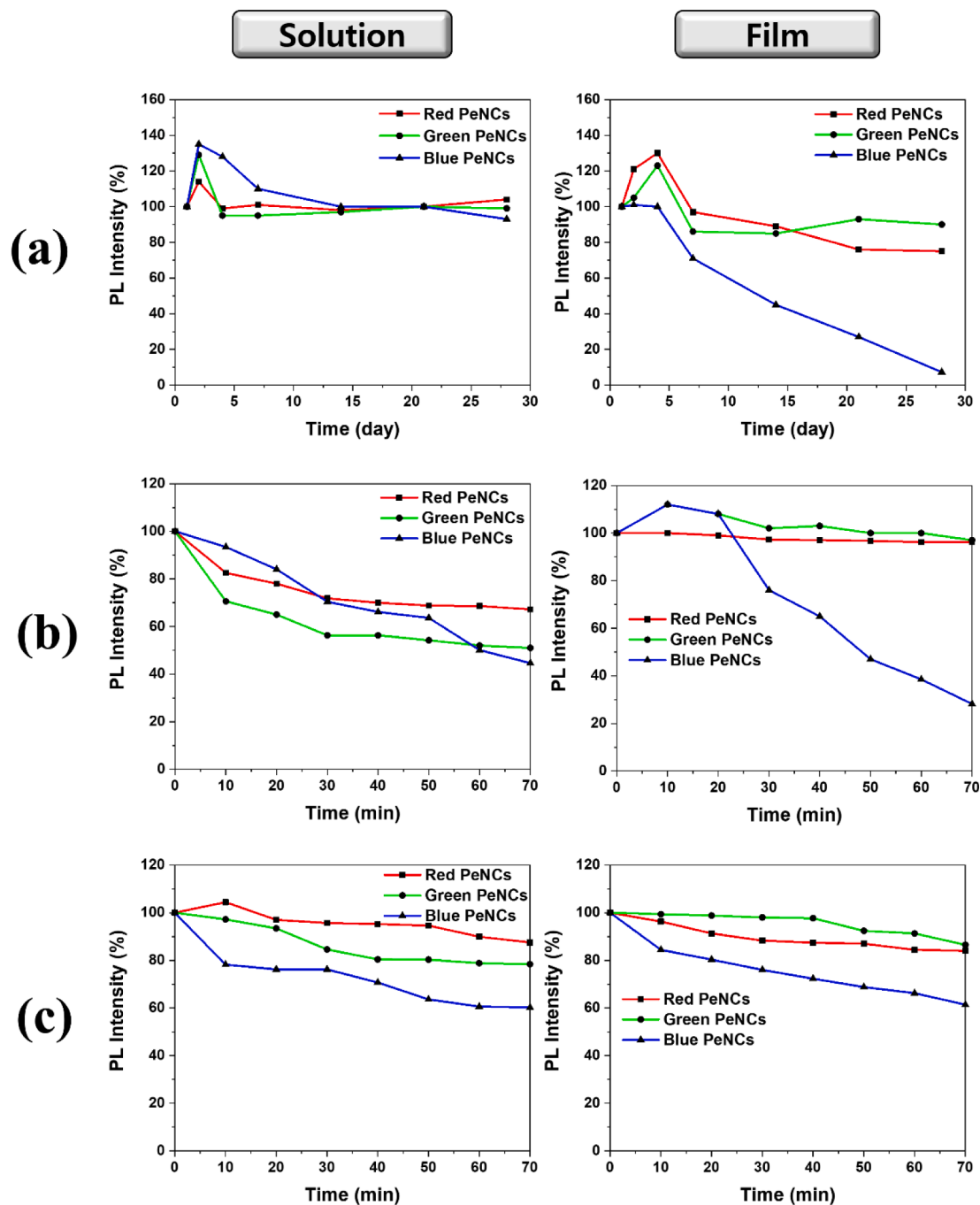


**Fig. 3.** The stability evaluation of prepared PeNCs: (a) long term stability (25 °C, 70 % humidity), (b) thermal stability (90 °C, 70 % humidity), and (c) UV light exposure stability.

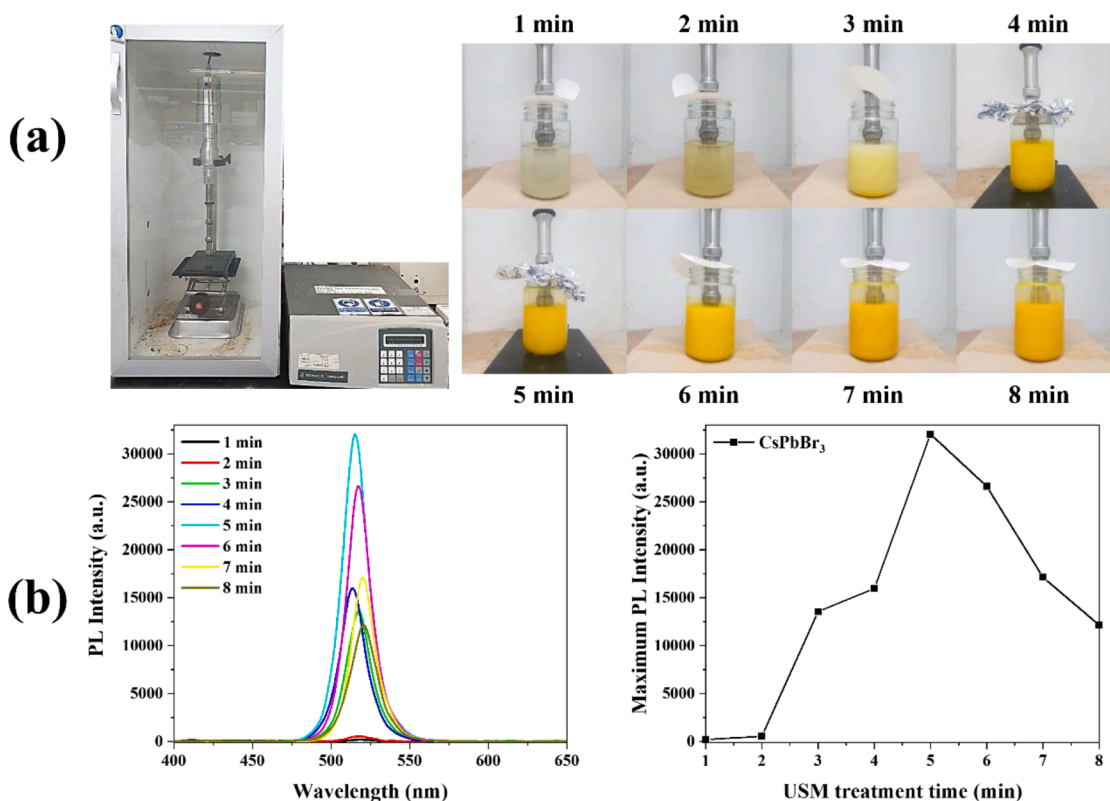


Fig. 4. (a) Photograph of ultrasonication equipment and the synthesis of large-capacity CsPbBr<sub>3</sub> PeNCs, and (b) The PL spectra intensity change according to ultrasonication treatment time.

intervals until the 28th day. All solution samples showed an increased PL intensity on the second and fourth days compared to the initial PL intensity, and the higher PL intensity was almost maintained or slightly decreased until the 28th day, exhibiting excellent long-term stability. In the case of film samples, the PL intensity of the red and green PeNCs was above 80 %, even after approximately-one month, whereas the intensity of the blue PeNCs decreased rapidly to 7.3 % compared to the initial intensity. As can be seen from the TEM image in Fig. 1e, black dots indicating surface defects were evenly distributed in the blue PeNCs, which is thought to decrease their stability [28]. The thermal stability of the RGB samples was evaluated using a hot plate at 90 °C for 70 min (Fig. 3b). All prepared RGB solution samples showed a decreasing trend compared to their initial intensities. After 70 min, the intensities of the red, green, and blue solutions were 67.2 %, 51 %, and 44.6 %, respectively, of the initial intensity. A decrease in PL strength with heating occurred because of structural decomposition of the PeNCs in solution originating from the residual ligands [30,38,39]. However, the film samples showed a relative intensity of more than 97 % for both red and green PeNCs, indicating very high thermal stability. The blue PeNC film sample showed a much lower relative intensity of 28.2 % mainly arises from their black dots. Finally, the prepared RGB samples were exposed to UV light (6 W, 610 μW/cm<sup>2</sup> at 365 nm) for 70 min to measure their photostability (Fig. 3c). The measured UV light stability showed a similar tendency to that of the thermal stability. Compared to the initial intensity after 70 min, the red PeNCs intensity was 89.9 %, green PeNCs intensity was 80.4 %, and blue PeNCs intensity was only 60.2 %. The film samples still showed high relative intensity of over 86 % for the red and green emissions, and 61.4 % for the blue emission. Consequently, the prepared red and green PeNCs showed excellent thermal and photostability, as well as ambient condition long-term stability, which is essential for PeNC/OLED hybrid device applications.

The scale-up synthesis of CsPbBr<sub>3</sub> PeNCs was successfully performed by large-capacity ultrasonicator, and the detailed synthetic photographs

were shown in Fig. 4a. The scale-up experiment was carried out by increasing the moles of the precursor and the solvents 25 times. The PL spectra intensity change according to ultrasonication treatment time was shown in Fig. 4b. The best treatment time for performing the maximum PL intensity was 5 min as shown in Fig. 4b, which is longer than the optimized reaction time (3.5 min) for lab scale synthesis. The maximum PL wavelength was slightly bathochromic shifted as the ultrasonication treatment time increased. If it was less than 5 min, the structure was not completely synthesized, and if it exceeded 5 min, the structure was collapsed due to excessive treatment time. Therefore, the wavelength and intensity of the emission peak may vary depending on the ultrasonic treatment time. The fluorescence intensity of the prepared scale-up PeNC solution exhibited almost the same value as that of lab scale synthesis if the reaction time was optimized.

We fabricated a hybrid PeNC/OLED device with PeNC inkjet ink as shown in Fig. 5. First, we fabricated a top-emitting blue OLED by considering the microcavity effect. The detailed procedure including the formulation of PeNC inkjet inks is described in the Experimental section. Inkjet-printing was performed with a Dimatix printer equipped with a 10 pL volume head at a voltage of 19 V and frequency of 1 kHz. More than 12 ink drops were stacked onto black bank patterns on a glass substrate. We improved our proficiency through repeated inkjet-printing experiments and improved the ink wettability through ink reforming. The width of the patterned pixels was 174 μm, the length was 50 μm, and the height of the pixel bank was 5.4 μm. The bank photoresist was prepared by mixing a lactam black millbase, acrylic binder polymer, multifunctional monomers, oxime ester-based photoinitiator, and PGMEA as a solvent. Bank patterns were fabricated using conventional photolithography processes. To obtain uniform hard CCLs, red and green PeNC inks were cured under 2000 mJ of UV light for 1 min. All photocuring processes were conducted under an inert atmosphere.

The rheological properties of the optimal red and green PeNC inkjet inks were analyzed. These inks were printed with a Dimatix inkjet

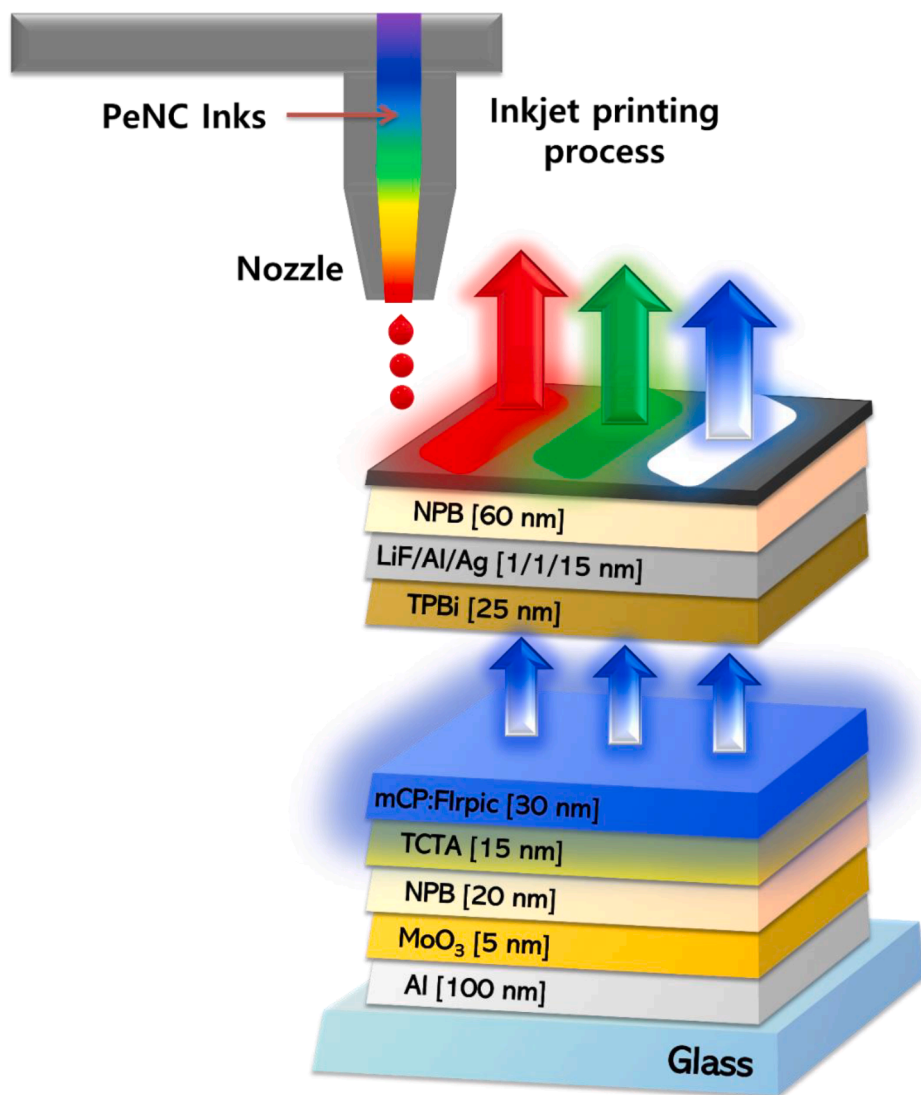


Fig. 5. The device structure of the blue OLED combining the perovskite CCLs with inkjet-printing.

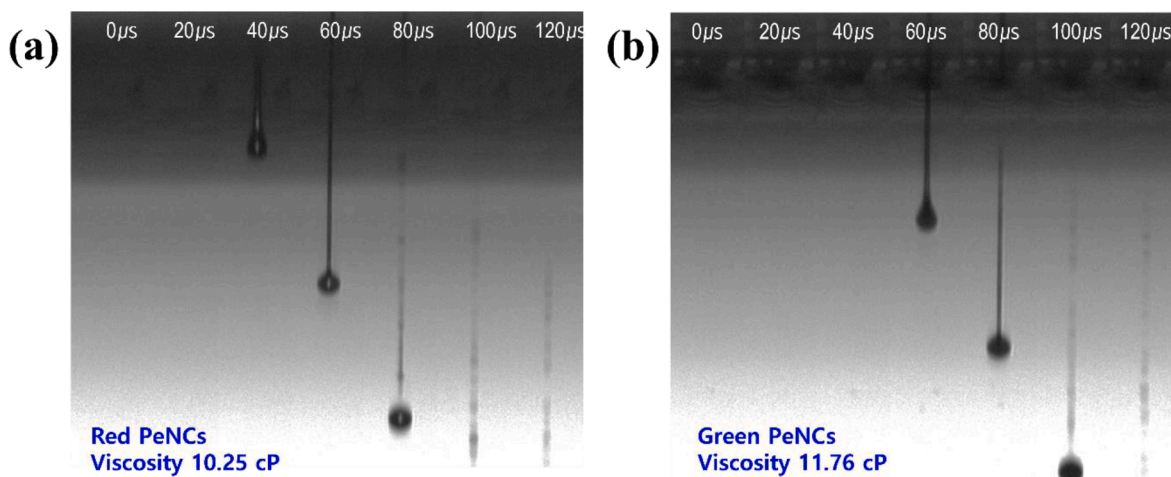


Fig. 6. The photographs of the jettability test of the prepared PeNC ink: (a) Red PeNCs and (b) Green PeNCs.

printer to observe the droplet formation of the inks and evaluate the jetting stability (Fig. 6). We observed the drop formation and fall shapes through a drop watcher. To be suitable inkjet inks, the viscosity and

surface tension at 25 °C should be controlled in the range of 1–12 cP and 20–70 mN/m, respectively [21,22]. The viscosity values of the formulated PeNC inks were both within the range suitable for inkjet-printing.

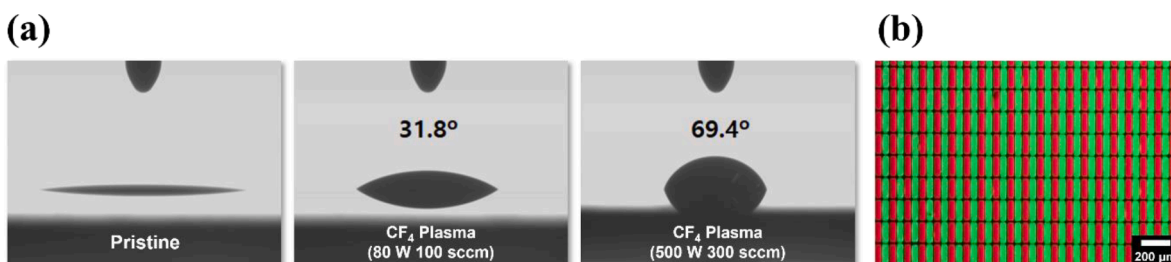


Fig. 7. The photographs of the (a) surface treatment of the substrate and (b) patterned array of the prepared PeNC inks.

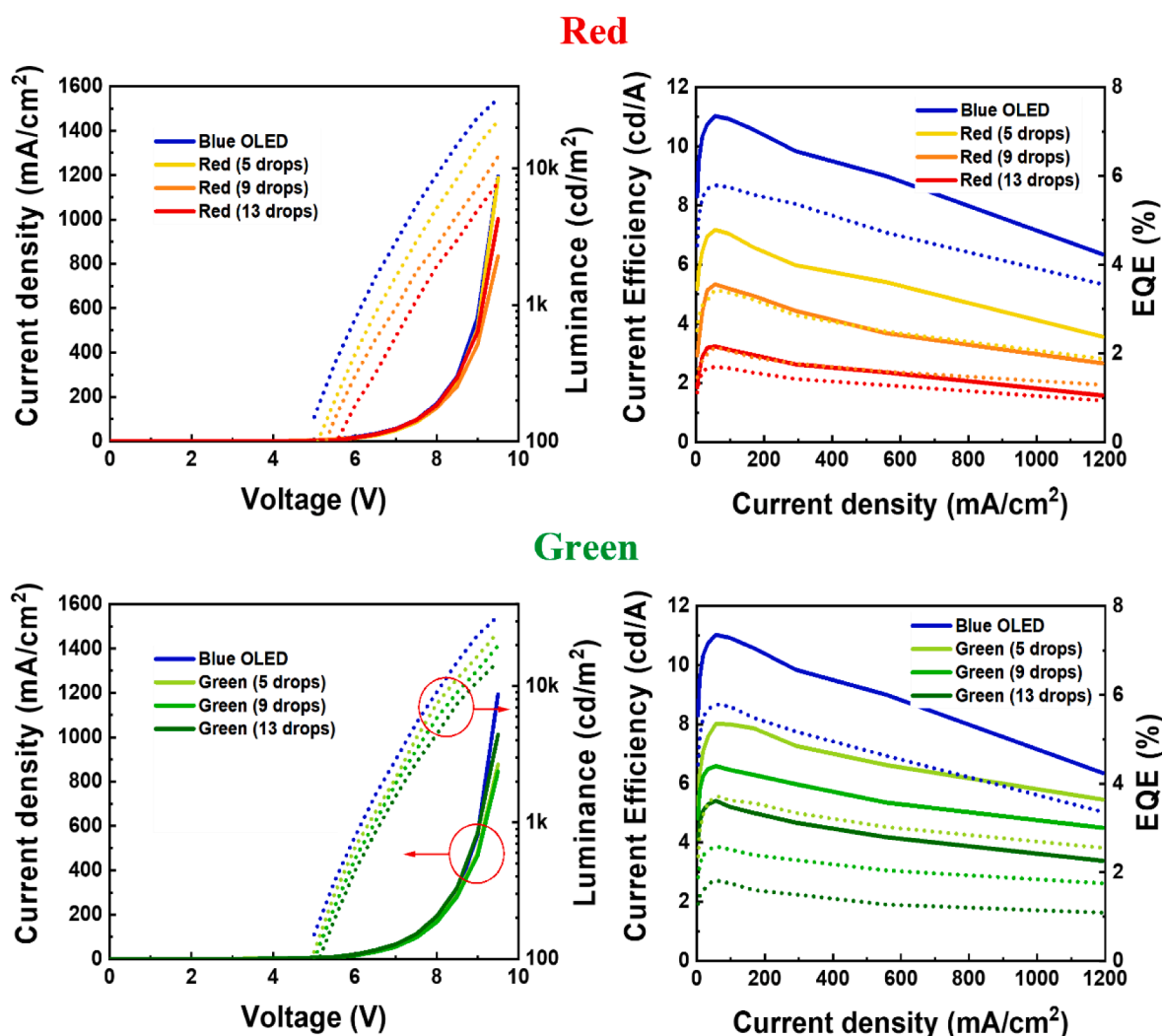


Fig. 8. The current density(J)-voltage(V)-luminance(L) curves of the blue OLED with different amounts of inkjet-printed drops of the PeNC CCLs.

The measured viscosity of the green PeNC ink was 11.76 cP, which was slightly higher than the 10.25 cP of the red PeNCs ink. We also optimized the firing voltage and frequency of the printer, where stable jetting of the prepared PeNC inks occurred at 19 V and 1 kHz. As shown in Fig. 6a, b, the ink printing tail of the droplet formed by the green PeNC ink was longer than that of the red PeNC ink. Because the viscosity of green PeNC ink is slightly higher, the droplets start falling more slower, and the tail is maintained longer. If the droplet discharge conditions are not optimized, satellite droplets or improper droplets are generated, deteriorating the print quality of the inkjet-printing process [21,40]. To ensure high-quality printing, the head drive voltage, drive waveform, and physical and rheological properties of the inks must be controlled. The

prepared red and green PeNC inks were found to have stable jetting and appropriate droplets, resulting in excellent printing performance.

We applied  $\text{CF}_4$  plasma treatment to the substrate to obtain sufficiently thick red and green CCLs to cut off the undesired blue OLED backlight. As shown in Fig. 7a, the contact angle between the untreated bank (pristine) and the  $\text{CF}_4$ -treated bank was measured. Because the conventional UV/ozone treatment increases hydrophilicity, the prepared PeNC inks did not form stable CCLs. Patterning errors occurred when the droplets climbed up the existing bank wall and invaded adjacent pixels [41,42]. We found that  $\text{CF}_4$  treatment lowered the surface energy of the banks and increased the hydrophobicity, thereby reducing the wettability of the PeNC inks. When the bank was treated

**Table 3**

The device characteristics of the fabricated PeNCs/OLED.

	Blue OLED	Green 5 drops	Green 9 drops	Green 13 drops	Red 5 drops	Red 9 drops	Red 13 drops
Luminance [ $\text{cd}/\text{m}^2$ ]	32,563	24,950	19,754	15,083	22,310	12,245	7,869
Current efficient [ $\text{cd}/\text{A}$ ]	11.0	8.01	6.58	5.41	7.18	5.33	3.23
EQE [%]	5.78	3.72	2.58	1.81	3.43	2.15	1.70
Coordination [x, y]	0.13, 0.08			0.09, 0.76			0.71, 0.29

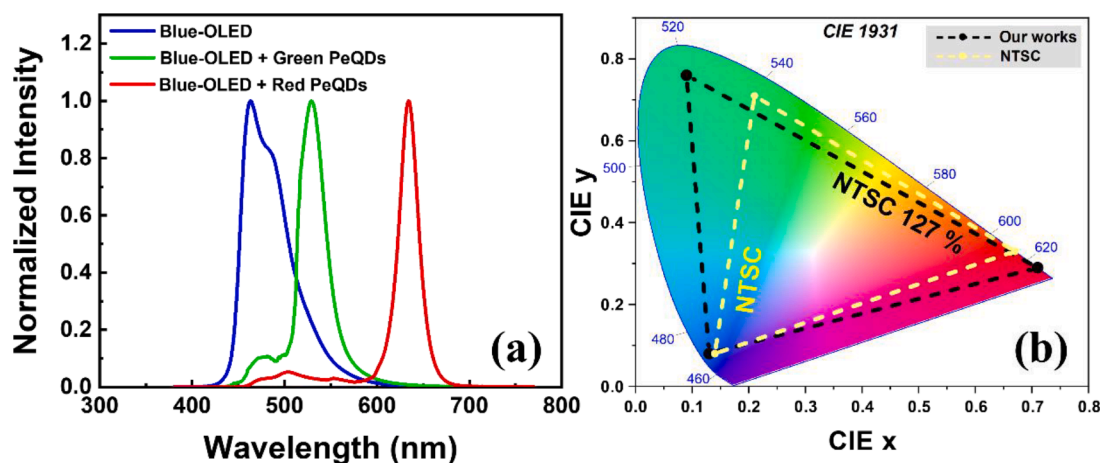


**Fig. 9.** (a) The EL spectra of blue OLED and the color conversion spectra of the green and red PeNC CCLs and (b) the color coordinate values compared with TV values.

with  $\text{CF}_4$  plasma at a power of 80 W and gas flow of 100 sccm, the contact angle of the ink was  $31.8^\circ$ . Because it was still difficult to form a stable layer, a contact angle of  $69.4^\circ$  was obtained by treatment at 500 W and 300 sccm. After sufficient coating of the bank wall and substrate surface with  $\text{CF}_4$  to increase hydrophobicity, inkjet-printing was successfully conducted to form stable thick CCLs (Fig. 7b). By adjusting the number of droplets of PeNC inks, the thickness of the CCL could be microcontrolled, and a sufficient CCL thickness exceeding the bank height was achieved using 13 drops.

Fig. 8 shows the current density (J)–voltage (V)–luminance (L) curves of the blue OLED and PeNC/OLED devices with inkjet-printed CCLs formed with various numbers of PeNC ink drops. The corresponding data are listed in Table 3. The maximum luminance, current efficiency, and external quantum efficiency (EQE) of the blue OLED were  $32,563 \text{ cd}/\text{m}^2$  (at 9.5 V),  $11.0 \text{ cd}/\text{A}$  (at 7 V), and 5.78 % (at 7 V), respectively. When the green perovskite CCL with five drops of PeNC ink was applied, the maximum luminance, current efficiency, and EQE were  $24,950 \text{ cd}/\text{m}^2$ ,  $8.01 \text{ cd}/\text{A}$ , and 3.72 %, respectively; increase the number of drops to 9 and 13, these values were  $24,950 \text{ cd}/\text{m}^2$ ,  $6.58 \text{ cd}/\text{A}$ , and 2.58 %, and  $15,083 \text{ cd}/\text{m}^2$ ,  $5.41 \text{ cd}/\text{A}$ , and 1.81 %, respectively (at the same voltages as the blue OLED). For 5 drops of the red PeNC ink, the maximum luminance, current efficiency, and EQE values were  $22,310 \text{ cd}/\text{m}^2$ ,  $7.18 \text{ cd}/\text{A}$ , and 3.43 %, respectively; as the number of drops increased to 9 and 13, these values were  $12,245 \text{ cd}/\text{m}^2$ ,  $5.33 \text{ cd}/\text{A}$ , and 2.15 %, and  $7,869 \text{ cd}/\text{m}^2$ ,  $3.23 \text{ cd}/\text{A}$ , and 1.70 %, respectively. As the thickness of the red and green CCL layers increased, their ability to block the blue light leakage and the color reproduction range improved, but the PeNC/OLED characteristics such as brightness and EQE degraded in a trade-off relationship [6,39]. More PeNC ink drops could be stably stacked in the pixels after the  $\text{CF}_4$  plasma treatment used in this study than achieved in previous studies. It is noted that even though a greater number of drops (13) were applied to thicken the red and green CCLs, the maximum luminance and EQE were still higher than those reported in our previous paper [6] because of the improved optical characteristics of the PeNC inks prepared in this study.

The electroluminescence (EL) spectra of the fabricated blue OLED and the green and red PL spectra converted by the prepared PeNC CCLs are shown in Fig. 9a. The undesired blue OLED leakage was almost suppressed in the green- and red-converted PL spectra. The color coordinate values of the inkjet-printed PeNC CCLs were measured using a M6100 J-V-L test system, and the comparison data with the National Television System Committee (NTSC) TV values are shown in Fig. 9b. The coordinates of the fabricated blue OLED backlights were (0.13, 0.08). The prepared green PeNC CCL had coordinates of (0.09, 0.76), and the red PeNC CCL had coordinates of (0.71, 0.29). The device samples exhibited a very wide color gamut, with vivid colors. The color reproduction range of the fabricated PeNC/OLED device was 27.3 % wider than that of the NTSC TV values. It was 10.3 % higher than that reported in our previous studies [6]. Compared with the results of other perovskite-based displays, our results particularly showed an improvement in the color reproduction range. This was because the synthesized PeNCs had outstanding optical properties and formed thick and stable CCLs through optimized inkjet-printing and  $\text{CF}_4$  surface treatment.

#### 4. Conclusion

In this study, we developed an optimized ultrasonication method for the high-capacity synthesis of highly luminescent inorganic PeNCs. We presented the polar-solvent-free and scalable single-step solution-phase synthesis of  $\text{CsPbBr}_3$  PeNCs with tunable bandgaps across the entire visible spectrum. After high-capacity synthesis of  $\text{CsPbBr}_3$  with a superior PLQY, halide anion exchange was performed to tune the stable emission wavelength. The crystal structures and morphologies of the prepared red, orange, green, cyan, and blue PeNCs were confirmed by FT-IR, XRD, and TEM analyses, respectively. The PeNCs had cubic crystal structures and hexagonal shapes with excellent optical properties, even without any being passivated. In particular, the maximum PL wavelengths of the red and green PeNCs after HIE were appropriate for LED applications, and their FWHMs were very narrow, showing outstanding color purity. The red PeNCs had the longest PL lifetime,

followed by the orange, green, cyan, and blue PeNCs. The prepared red and green PeNCs also showed excellent thermal and UV exposure stability, as well as long-term stability, which is essential for PeNC/OLED hybrid device applications. The prepared PeNC solutions were formulated into uniformly stable inks containing a photocuring agent with appropriate additives. The physical and rheological properties of the PeNC inks were optimized, and a CF<sub>4</sub> plasma treatment was conducted to enable successful inkjet-printing. By adjusting the number of printed droplets of the PeNC inks, the thickness of the CCL was microcontrolled, and a sufficient CCL thickness exceeding the bank height was achieved using 13 drops. Finally, we fabricated a hybrid PeNC/OLED device based on the synthesized red and green PeNCs using optimized ultrasonication and HIE methods. The color reproduction range of the fabricated devices was 27.3 % wider than that of the NTSC TV values, expressing very vivid colors.

### Declaration of Competing Interest

The authors declare that they have no known competing financial interests or personal relationships that could have appeared to influence the work reported in this paper.

### Data availability

Data will be made available on request.

### Acknowledgement

This work was supported by the Material & Component Technology Development Program (20021893, Development of highly bright formaldehyde free type daylight fluorescent resin pigments with a size less than 200 nm and commercialization technology) funded by the Ministry of Trade, Industry and Energy.

### References

- L.N. Quan, B.P. Rand, R.H. Friend, S.G. Mhaisalkar, T.-W. Lee, E.H. Sargent, Perovskites for next-generation optical sources, *Chemical Reviews* 12 (2019) 7444–7477.
- Q.A. Akkerman, M. Gandini, F. Di Stasio, P. Rastogi, F. Palazon, G. Bertoni, J. M. Ball, M. Prato, A. Petrozza, L. Manna, Strongly Emissive Perovskite Nanocrystal Inks for High-Voltage Solar Cells, *Nature Energy* 2 (2016) 16194.
- F. Zhou, Z. Li, H. Chen, Q. Wang, L. Ding, Z. Jin, Application of Perovskite Nanocrystals (NCs)/Quantum Dots (QDs) in Solar Cells, *Nano Energy* 73 (2020), 104757.
- G. Hong, J. Li, Z. Su, X. Li, S. Li, J. Sun, F. Liu, Y. Liu, In-Situ Sintered CsPbBr<sub>3</sub>/CsPb<sub>2</sub>B<sub>5</sub> Perovskite Nanocrystals into Mesoporous Silica for White High-Efficiency LEDs, *Journal of Solid State Chemistry* 310 (2022), 123032.
- F. Xu, D. Chen, D. Huang, K. Xu, S. Liang, J. Hu, X. Zhang, L. Liu, F. Xiong, H. Zhu, Suppression of Photoinduced Phase Segregation in Mixed-Halide Perovskite Nanocrystals for Stable Light-Emitting Diodes, *The Journal of Physical Chemistry Letters* 13 (2022) 718–725.
- S.Y. Lee, G. Lee, D.Y. Kim, S.H. Jang, I. Choi, J. Park, H.-K. Park, J.W. Jung, K. H. Cho, J. Choi, Investigation of High-Performance Perovskite Nanocrystals for Inkjet-Printed Color Conversion Layers with Superior Color Purity, *APL Photonics* 6 (2021), 056104.
- H. Algadi, A. Umar, H. Albarqi, T. Alsuwian, S. Baskoutas, Carbon Nanodots as a Potential Transport Layer for Boosting Performance of All-Inorganic Perovskite Nanocrystals-Based Photodetector, *Crystals* 11 (2021) 717.
- Y. Che, X. Cao, Y. Zhang, J. Yao, High-Performance Photodetector Using CsPbBr<sub>3</sub> Perovskite Nanocrystals and Graphene Hybrid Channel, *Journal of Materials Science* 56 (2020) 2341–2346.
- C. Zhao, J. Tao, J. Tian, G. Weng, H. Liu, Y. Liu, J. Yan, S. Chen, Y. Pan, X. Hu, et al., High Performance Single-Mode Vertical Cavity Surface Emitting Lasers Based on CsPbBr<sub>3</sub> Nanocrystals with Simplified Processing, *Chemical Engineering Journal* 420 (2021), 127660.
- Z. Qin, C. Zhang, L. Chen, T. Yu, X. Wang, M. Xiao, Electrical Switching of Optical Gain in Perovskite Semiconductor Nanocrystals, *Nano Letters* 21 (2021) 7831–7838.
- S. Feldmann, M.K. Gangishetty, I. Bravić, T. Neumann, B. Peng, T. Winkler, R. H. Friend, B. Monserrat, D.N. Congreve, F. Deschler, Charge Carrier Localization in Doped Perovskite Nanocrystals Enhances Radiative Recombination, *Journal of the American Chemical Society* 143 (2021) 8647–8653.
- Lan, L.; Zou, J.; Jiang, C.; Liu, B.; Wang, L.; Peng, J. Inkjet Printing for Electroluminescent Devices: Emissive Materials, Film Formation, and Display Prototypes. (10), *Frontiers of Optoelectronics*, (2017), 329–352.
- Y. Tong, E. Bladt, M.F. Aygüler, A. Manzi, K.Z. Milowska, V.A. Hintermayr, P. Docampo, S. Bals, A.S. Urban, L. Polavarapu, et al., Highly Luminescent Cesium Lead Halide Perovskite Nanocrystals with Tunable Composition and Thickness by Ultrasonication, *Angewandte Chemie International Edition* 55 (2016) 13887–13892.
- L. Protesescu, S. Yakunin, M.I. Bodnarchuk, F. Krieg, R. Caputo, C.H. Hendon, R. X. Yang, A. Walsh, M.V. Kovalenko, Nanocrystals of Cesium Lead Halide Perovskites (CsPbX<sub>3</sub>, X = Cl, Br, and I): Novel Optoelectronic Materials Showing Bright Emission with Wide Color Gamut, *Nano Letters* 15 (2015) 3692–3696.
- M.V. Kovalenko, L. Protesescu, M.I. Bodnarchuk, Properties and Potential Optoelectronic Applications of Lead Halide Perovskite Nanocrystals, *Science* 358 (2017) 745–750.
- A. Wang, X. Yan, M. Zhang, S. Sun, M. Yang, W. Shen, X. Pan, P. Wang, Z. Deng, Controlled Synthesis of Lead-Free and Stable Perovskite Derivative Cs<sub>2</sub>SnI<sub>6</sub> Nanocrystals via a Facile Hot-Injection Process, *Chemistry of Materials* 28 (2016) 8132–8140.
- Sun, S.; Yuan, D.; Xu, Y.; Wang, A.; Deng, Z. Ligand-Mediated Synthesis of Shape-Controlled Cesium Lead Halide Perovskite Nanocrystals via Reprecipitation Process at Room Temperature. (10), *ACS Nano*, (2016), 3648–3657.
- F. Zhang, S. Huang, P. Wang, X. Chen, S. Zhao, Y. Dong, H. Zhong, Colloidal Synthesis of Air-Stable CH<sub>3</sub>NH<sub>3</sub>PbI<sub>3</sub> Quantum Dots by Gaining Chemical Insight into the Solvent Effects, *Chemistry of Materials* 29 (2017) 3793–3799.
- Zhong, Q.; Cao, M.; Hu, H.; Yang, D.; Chen, M.; Li, P.; Wu, L.; Zhang, Q. One-Pot Synthesis of Highly Stable CsPbBr<sub>3</sub>@SiO<sub>2</sub> Core-Shell Nanoparticles. (12), *ACS Nano*, (2018), 8579–8587.
- X. He, S. Li, G. Cao, J. Hu, J. Zhang, R. Qiao, J. Pan, G. Shao, In Situ Atomic-Scale Engineering of the Chemistry and Structure of the Grain Boundaries Region of Li<sub>3-x</sub>La<sub>2/3-x</sub>TiO<sub>3</sub>, *Scripta Materialia* 185 (2020) 134–139.
- S. Choi, S.Y. Lee, D.Y. Kim, H.-K. Park, M.J. Ko, K.H. Cho, J. Choi, The Synthesis and Characterisation of the Highly Stable Perovskite Nano Crystals and Their Application to Ink-Jet Printed Colour Conversion Layers, *Journal of Industrial and Engineering Chemistry* 85 (2020) 226–239.
- B. Derby, Inkjet Printing of Functional and Structural Materials: Fluid Property Requirements, Feature Stability, and Resolution, *Annual Review of Materials Research* 40 (2010) 395–414.
- Y. Altintas, I. Torun, A.F. Yazici, E. Beskazak, T. Erdem, M. Serdar Onses, E. Mutlugun, Multiplexed Patterning of Cesium Lead Halide Perovskite Nanocrystals by Additive Jet Printing for Efficient White Light Generation, *Chemical Engineering Journal* 380 (2020), 122493.
- Y. Ida, Interionic Repulsive Force and Compressibility of Ions, *Physics of the Earth and Planetary Interiors* 13 (1976) 97–104.
- S. Cho, S.H. Yun, Poly(Catecholamine) Coated CsPbBr<sub>3</sub> Perovskite Microlasers: Lasing in Water and Biofunctionalization, *Advanced Functional Materials* 31 (2021) 2101902.
- J. Wu, S. Zhao, X. Chi, N. Sui, Z. Kang, Q. Zhou, H. Zhang, X. Li, B. Zhao, Y. Wang, Optical Property of Inorganic Halide Perovskite Hexagonal Nanocrystals, *The Journal of Physical Chemistry C* 125 (2021) 25044–25054.
- J. Ban, X. Wen, H. Lei, G. Cao, X. Liu, C. Niu, G. Shao, J. Hu, In-Plane Grain Boundary Induced Defect State in Hierarchical NiCo-LDH and Effect on Battery-Type Charge Storage, *Nano Research* (2022).
- M. Benavides-Garcia, K. Balasubramanian, Bond Energies, Ionization Potentials, and the Singlet-Triplet Energy Separations of SnCl<sub>2</sub>, SnBr<sub>2</sub>, SnI<sub>2</sub>, PbCl<sub>2</sub>, PbBr<sub>2</sub>, PbI<sub>2</sub>, and Their Positive Ions, *The Journal of Chemical Physics* 100 (1994) 2821–2830.
- Nedelcu, G.; Protesescu, L.; Yakunin, S.; Bodnarchuk, M. I.; Grotevent, M. J.; Kovalenko, M. V. Fast Anion-Exchange in Highly Luminescent Nanocrystals of Cesium Lead Halide Perovskites (CsPbX<sub>3</sub>, X = Cl, Br, I). (15), *Nano Letters*, (2015), 5635–5640.
- S.-W. Dai, Y.-L. Lai, L. Yang, Y.-T. Chuang, G.-H. Tan, S.-W. Shen, Y.-S. Huang, Y.-C. Lo, T.-H. Yeh, C.-I. Wu, et al., Organic Lead Halide Nanocrystals Providing an Ultra-Wide Color Gamut with Almost-Unity Photoluminescence Quantum Yield, *ACS Applied Materials & Interfaces* 13 (2021) 25202–25213.
- H. Liu, Z. Wu, H. Gao, J. Shao, H. Zou, D. Yao, Y. Liu, H. Zhang, B. Yang, One-Step Preparation of Cesium Lead Halide CsPbX<sub>3</sub> (X = Cl, Br, and I) Perovskite Nanocrystals by Microwave Irradiation, *ACS Applied Materials & Interfaces* 9 (2017) 42919–42927.
- S. Wang, Y. Wang, Y. Zhang, X. Zhang, X. Shen, X. Zhuang, P. Lu, W.W. Yu, S. V. Kershaw, A.L. Rogach, Cesium Lead Chloride/Bromide Perovskite Quantum Dots with Strong Blue Emission Realized via a Nitrate-Induced Selective Surface Defect Elimination Process, *The Journal of Physical Chemistry Letters* 10 (2018) 90–96.
- A. De, S. Das, N. Mondal, A. Samanta, Highly Luminescent Violet- and Blue-Emitting Stable Perovskite Nanocrystals, *ACS Materials Letters* 1 (2019) 116–122.
- E.V. Ushakova, S.A. Cherevkov, V.A. Kuznetsova, A.V. Baranov, Lead-Free Perovskites for Lighting and Lasing Applications: A Minireview, *Materials* 12 (2019) 3845.
- Y. Tong, E.-P. Yao, A. Manzi, E. Bladt, K. Wang, M. Döblinger, S. Bals, P. Müller-Buschbaum, A.S. Urban, L. Polavarapu, et al., Spontaneous Self-Assembly of Perovskite Nanocrystals into Electronically Coupled Supercrystals: Toward Filling the Green Gap, *Advanced Materials* 30 (2018) 1801117.
- X. Li, Y. Wang, H. Sun, H. Zeng, Amino-Mediated Anchoring Perovskite Quantum Dots for Stable and Low-Threshold Random Lasing, *Advanced Materials* 29 (2017) 1701185.

- [37] J. He, A.S. Vasenko, R. Long, O.V. Prezhdo, Halide Composition Controls Electron-Hole Recombination in Cesium-Lead Halide Perovskite Quantum Dots: A Time Domain Ab Initio Study, *The Journal of Physical Chemistry Letters* 9 (2018) 1872–1879.
- [38] Y.S. Shin, Y.J. Yoon, K.T. Lee, W. Lee, H.S. Kim, J.W. Kim, H. Jang, M. Kim, D. S. Kim, G.-H. Kim, et al., High-Performance Perovskite Light-Emitting Diodes with Surface Passivation of CsPbBr<sub>x</sub>I<sub>3-x</sub> Nanocrystals via Antisolvent-Triggered Ion-Exchange, *ACS Applied Materials & Interfaces* 12 (2020) 31582–31590.
- [39] L. Rao, Y. Tang, C. Song, K. Xu, E.T. Vickers, S. Bonabi Naghadeh, X. Ding, Z. Li, J. Z. Zhang, Polar-Solvent-Free Synthesis of Highly Photoluminescent and Stable CsPbBr<sub>3</sub> Nanocrystals with Controlled Shape and Size by Ultrasonication, *Chemistry of Materials* 31 (2018) 365–375.
- [40] Y.M. Jo, S.-J. Park, Experimental Analysis of Droplet Formation Process for Inkjet Printhead, *ILASS-Korea* 15 (2010) 163–169.
- [41] T. Xuan, S. Shi, L. Wang, H.-C. Kuo, R.-J. Xie, Inkjet-Printed Quantum Dot Color Conversion Films for High-Resolution and Full-Color Micro Light-Emitting Diode Displays, *The Journal of Physical Chemistry Letters* 11 (2020) 5184–5191.
- [42] D.Y. Kim, Y.J. Han, J. Choi, C. Sakong, B.-K. Ju, K.H. Cho, Inkjet Printed Quantum Dot Film Formed by Controlling Surface Wettability for Blue-to-Green Color Conversion, *Organic Electronics* 84 (2020), 105814.